Carbon 232 (2025) 119802

Contents lists available at ScienceDirect

Carbon

journal homepage: www.elsevier.com/locate/carbon

Disordering of graphene nanoplatelet, carbon nanotube and C_{60} fullerene under shear stress

Yi Yang [a,b], Mingzhi Yuan [a,b,*], Chao Qian [b,c], Chengyu Li [b], Yanping Yang [b], Xueyan Du [b], Hongliang Dong [b,d], Bin Chen [a,b,d,**]

[a] School of Science, Harbin Institute of Technology, Shenzhen, 518055, China
[b] Center for High Pressure Science & Technology Advanced Research (HPSTAR), Shanghai, 201203, China
[c] School of Energy and Materials, Shanghai Polytechnic University, Shanghai, 201209, China
[d] Shanghai Key Laboratory of Material Frontiers Research in Extreme Environments (MFree), Institute for Shanghai Advanced Research in Physical Sciences (SHARPS), Shanghai, 201203, China

ARTICLE INFO

Keywords:
Carbon nanomaterials
High pressure
Shear stress
sp^2-sp^3
Amorphous carbon

ABSTRACT

Carbon nanomaterials typically possess excellent mechanical properties, enabling them to withstand extreme physical environments. However, the response of different nanostructures under shear stress has not yet been experimentally investigated. In this study, we employ the rotational diamond anvil cell to apply pressure and shear to three carbon nanomaterials–graphene nanoplatelet, multi-wall carbon nanotube and C_{60} fullerene–and investigate their structure evolution using Raman spectroscopy and electron microscopy. Detailed analysis revealed that the materials exhibit distinct changes in their intrinsic structure. Specifically, defects and lattice distortion were introduced into graphene nanoplatelet, carbon nanotube broke down into curly graphene fragments, and C_{60} completely transformed into amorphous carbon. The most compelling discovery is the remarkably high degree of amorphization process in C_{60} at room temperature, accompanied by an sp^3 hybridization fraction reaching 20.84 %. Our results underscore the profound impact of shear stress on the stability of carbon-based nanomaterials, provide new insights into their mechanical behavior and potential limitation in practical application, and offer a strategy for regulating these materials which have the strongest covalent bonds.

1. Introduction

Carbon materials have long captivated researchers due to their exceptional physical properties. Graphene, for instance, boasts a Young's modulus of approximately 1 TPa and an intrinsic strength of around 130 GPa [1]. Incorporating graphene into coatings has been shown to significantly enhance mechanical properties [2]. The epoxy resin composites with graphene and graphite exhibited varying degrees of improvement in Young's modulus and tensile strength. Additionally, the graphene-epoxy resin composites demonstrated a superior ability to retard crack propagation [3]. Similarly, carbon nanotube (CNT) exhibits impressive toughness, capable of withstanding internal pressures up to about 40 GPa [4]. Calculations show that the C_{60} molecule can return to spherical shape after being subjected to high strain [5]. These studies underscore the significant potential of carbon materials in the field of structural applications. Further advancements in current methodologies to precisely manipulate these carbon materials could lead to the effective utilization of them.

High pressure has been closely intertwined with the study of carbon materials. Earlier studies have gained detailed understanding of the behavior of graphite under high pressure. Approximately half of the π bonds converting to σ bonds has been found in compressed graphite at room temperature. Additionally, due to the extreme hardness of the new phase of graphite, shallow indentations were left on the diamond anvils [6]. Study have indicated that under high shear stress, few-layer-graphene may transform into disordered carbon nanoclusters and amorphous carbon [7]. A hexagonal carbon phase has been discovered in cold-compressed CNT at ~75 GPa, which can be quenched at ambient pressure. This phase was hard enough to leave significant cracks on the diamond anvil [8]. Chen et al. observed the formation of carbon nanoribbons in cold-compressed CNT [9]. For C_{60} fullerene, its changes under extreme conditions are also of great interest. Previous

* Corresponding author. School of Science, Harbin Institute of Technology, Shenzhen, 518055, China.
** Corresponding author. School of Science, Harbin Institute of Technology, Shenzhen, 518055, China.
E-mail addresses: mingzhi.yuan@hpstar.ac.cn (M. Yuan), chenbin@hpstar.ac.cn (B. Chen).

https://doi.org/10.1016/j.carbon.2024.119802
Received 6 September 2024; Received in revised form 23 October 2024; Accepted 4 November 2024
Available online 5 November 2024

reports have already provided evidence of the existence of an ultrahard phase in C_{60} under high shear stress [10–13]. Paracrystalline diamond has been synthesized by subjecting C_{60} to controlled high-temperature and high-pressure conditions [14]. At moderate pressure and temperature, Zhang et al. found that C_{60} transformed into amorphous carbon that is both hard and tough, with a bandgap of 0.1–0.3 eV [15]. Recent studies on carbon have highlighted the critical role of high shear stress, suggesting that it can substitute for high-temperature treatment [16–18]. Understanding the behavior of carbon materials under extreme conditions, particularly high shear stress, is crucial for controlling them effectively. However, the shear responses of graphene nanoplatelet (GNP), CNT and C_{60} have yet to be directly compared in detail.

This study aims to fill the gap by employing a rotational diamond anvil cell (rDAC) to subject GNP, CNT, and C_{60} to high shear stress. By examining the structural changes using Raman spectroscopy and electron microscopy, we seek to elucidate how shear stress influences these materials at the nanoscale. Such insights not only advance fundamental research but also pave the way for engineering applications requiring precise manipulation of the structure of carbon nanomaterials.

2. Materials and methods

2.1. Sample preparation

The structure of starting materials GNP (XFNANO), CNT and C_{60} (Macklin Biochemical Technology) powders was checked using transmission electron microscopy (TEM). In the high resolution transmission electron microscopy (HRTEM) image of the pristine GNP, a distinct lattice fringe corresponding to the (001) of graphite is observed, with an interplanar spacing of approximately 0.335 nm (Fig. 1a) and a sheet size of 3–5 μm. The HRTEM image of the CNT, as shown in Fig. 1b, reveals that the nanotube walls consist of around 15 layers, with an interlayer spacing of approximately 0.338 nm. The HRTEM image and corresponding selected area electron diffraction (SAED) pattern show good crystallinity of the original C_{60} (Fig. 1c). High pressure and shear were applied to the three samples using an rDAC (Fig. 1d). The three samples were loaded into the sample chamber without any pressure transmitting medium. To minimize the introduction of dispersed impurities into the samples during torsion, which could affect subsequent characterization, we estimated the applied pressure by monitoring the Raman shift of stressed diamond anvil [19]. In the shear experiments, the samples were compressed to about 20 GPa, and one of the diamond anvils was rotated by 360° while maintaining a constant axial force. Each sample also underwent a control experiment where only pressure was applied and no rotation of anvil was operated. The shear process was completed in three steps, each with a rotation angle of 120°. We have compiled the collected pressure data during the shear process in Fig. S1. When the samples were GNP and CNT, the pressure increased after rotation. However, for C_{60}, the pressure decreased after rotation. Previous reports have mentioned the volumetric effect of C_{60} under high pressure, which we believe is the main reason for the pressure drop [20,21]. The uneven pressure distribution in the chamber indicated that the sample generated significant friction with the anvil surfaces. Finally, all samples were decompressed to ambient pressure for further characterizations.

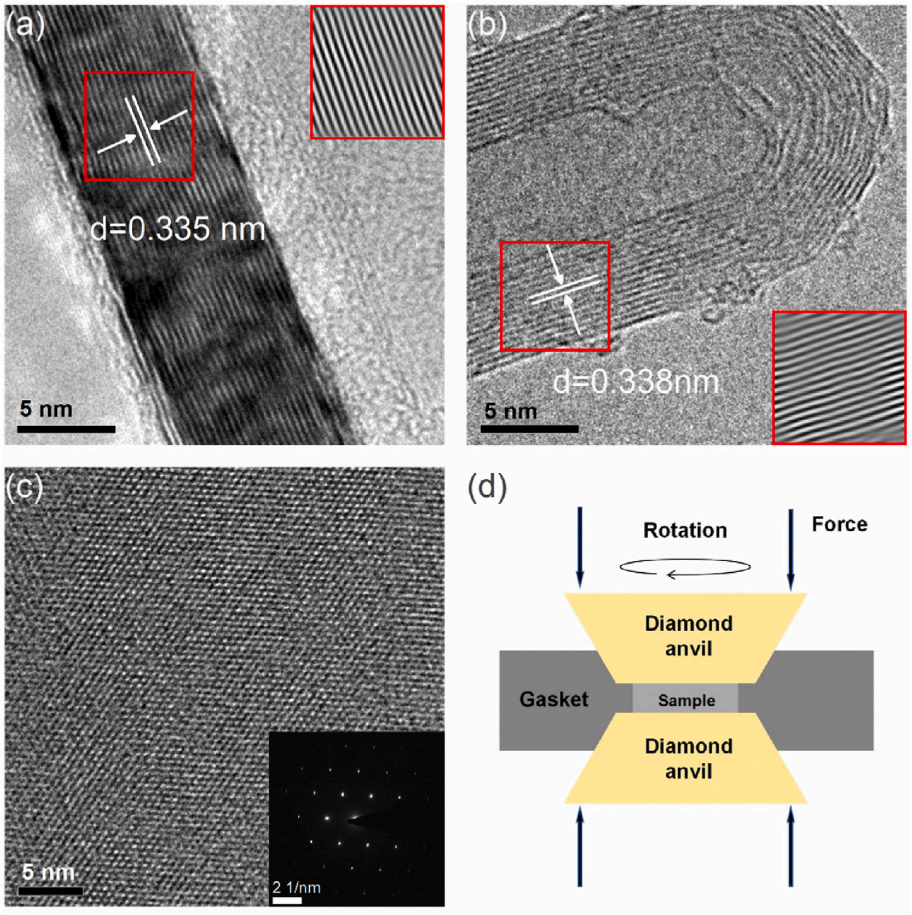

Fig. 1. HRTEM images of the original GNP (a), CNT (b), and C_{60} (c). Insets in (a) and (b) demonstrate the corresponding inverse fast Fourier transform results in the red boxes. Inset in (c) shows the SAED pattern of the C_{60} crystal. (d) A schematic of the core part of the rDAC set up. High pressure was generated by pressing two opposite diamond anvils against each other, and shear was induced by rotating the top anvil. Pre-indented stainless steel gaskets were used in the experiments. (For interpretation of the references to colour in this figure legend, the reader is referred to the Web version of this article.)

2.2. Raman spectroscopy

Raman spectroscopy is one of the most efficient and widely used methods for nondestructive characterization of carbon materials. All Raman spectra were collected using the Renishaw inVia Raman system with a 532 nm excitation laser. Measurements were performed with an incident laser power below 0.4 mW to avoid sample damage or laser-induced heating effect. Due to varying stress states in the sample chamber of the rDAC, representative Raman spectra were collected at two different positions A and B. Position A is located at the center of the sample chamber, and position B is at the periphery, ~75 μm away from the center (Fig. S2). Line scans were performed along the diameter of the sample chamber.

2.3. TEM-electron energy loss spectroscopy (EELS)

Lamellae were cut from position B with smooth surfaces in the recovered samples (Fig. S3) using an FEI Versa 3D focused ion beam system for TEM observation. Prior to slicing, a layer of Pt was deposited on the sample surface as the protective coating material. The thickness of the lamellae was reduced to ~70 nm using the ion beam with low current to assure good quality of the TEM imaging.

TEM characterization was conducted on a Titan Cubed Themis G2 microscope operating at 300 kV equipped with a Gatan Imaging Filter to enable electron energy loss spectroscopy to be performed.

3. Results and discussion

We initially analyzed the Raman spectra of the original samples, as illustrated in Fig. 2. The Raman spectrum of pristine GNP exhibits a peak at 1352 cm^{-1}, commonly referred to as the D-band, whose intensity is related to defects in the sample [22]. A sharp G-peak can be clearly observed at 1580 cm^{-1}, which is characteristic of the sp^2 hybridized carbon atoms. Attached to the right side of the G-band is the D′-band observed around 1620 cm^{-1}, whose intensity is correlated with that of the D-band, as it also originates from defects in the sample [15]. In the Raman spectrum of pristine CNT, a remarkably strong D-band can be observed, with its intensity exceeding that of the G-band, and the intensity of the D′-band is approaching that of the G-band. This indicates a very high density of defects within the CNT sample [23]. The strongest Raman peak of the original C_{60} at 1469 cm^{-1} is the A_g mode, which is caused by the longitudinal vibration of the double bonds between pentagons. For the uniaxially compressed samples, where the anvil was not rotated, both GNP and CNT exhibited minimal changes in their Raman spectra (Fig. 2a and c). Under high pressure, new covalent bonds may form between the layers of GNP and CNT, leading to weakening of the G band [6]. Our results confirm that this transformation is reversible below 20 GPa. In contrast, the Raman spectra of the C_{60} powders

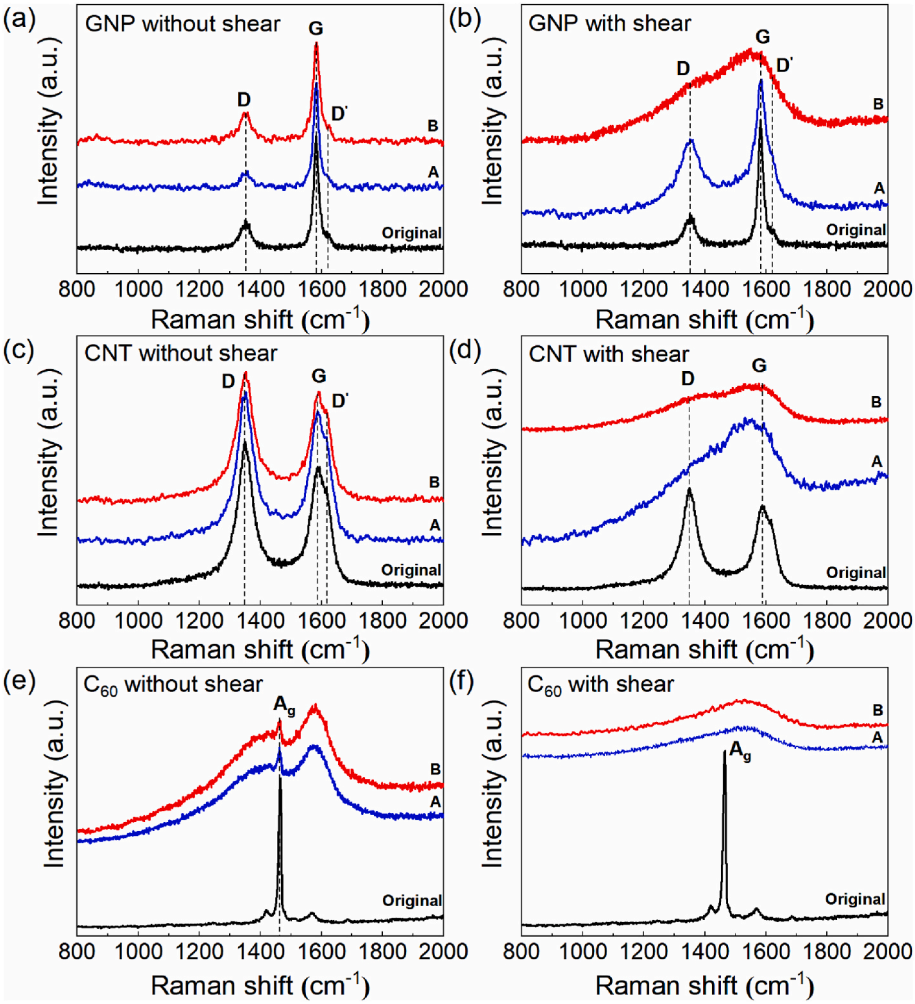

Fig. 2. Raman spectra of CNP, CNT and C_{60} fullerene recovered from high pressure of 20 GPa (a, c, e) and from high pressure of 20 GPa and shear (b, d, f). The black spectra represent the signals of the original samples, while blue and red spectra correspond to the signals from positions A and B within the sample chamber, respectively. The dashed lines and letter labels indicate the corresponding Raman characteristic bands. (For interpretation of the references to colour in this figure legend, the reader is referred to the Web version of this article.)

recovered from the same pressure display a notable weakening of the A_g mode signal (Fig. 2e). Additionally, the broader peaks associated with disordered carbon are observed at positions A and B. It has been reported that the Raman and XRD signals of C_{60} will weaken under 20 GPa, due to the collapse of C_{60} molecules or the formation of new intermolecular covalent bonds [24–27]. These changes are not reversible after compression to 20 GPa. C_{60} may have undergone a partial loss of crystallinity due to compression. This also suggests that the C_{60} is relatively sensitive to pressure even without significant shear stress.

Subsequently, we analyzed the Raman spectra of the samples subjected to high shear stress. The GNP powders recovered from 20 GPa to 360° of shear were examined using the same Raman measurements, as shown in Fig. 2b. Notably, the spectrum at position A still exhibits distinct but broadened D- and G-bands, indicating a reduction in crystallinity. However, at position B, the D- and G-bands become broader, and the F-band, associated with the vibrations of pentagon carbon rings, appeared at ~1450 cm^{-1} [28]. This suggests a more significant structure alteration at the periphery of the chamber compared to the center. Comparison of the Raman spectra from positions A and B of the CNT powders before and after shear treatment is presented in Fig. 2d. It is clear that the spectra at both A and B positions have undergone substantial changes, becoming markedly different from those of the pristine sample. The distinct features of the G-band and D-band are no longer observable, indicating a significant disruption of the original structure. The signal at A in CNT is similar to that at B in the sheared GNP, where the D- and G-band are nearly merged, resembling the characteristics of most disordered carbon. The signal at position B exhibited overall weaker intensity. However, for the C_{60} recovered from high pressure and shear, the Raman signals at positions A and B are identical. As shown in Fig. 2f, the sharp A_g peak is completely absent. Instead, the spectra at both positions A and B in the chamber display a similar broad hump ranging from 1000 cm^{-1}–1700 cm^{-1}, with no discernible peak features. This spectral shape is reminiscent of that observed in C_{60} quenched from 12.5 GPa to 550 °C using large volume press, which is highly disordered carbon [15].

The point measurements of the aforementioned samples revealed significant variations in Raman spectra at different radial positions, corresponding to regions subjected to varying degrees of shear stress. To further illustrate the relationship between shear stress and structure changes, we performed line scans across the sample chamber, as shown in Fig. S2, with a step size of 5 μm. Tuinstra and Koenig originally established a relationship between the reciprocal of the crystallite size L_a, calculated from XRD data, and the intensity ratio of D-band and G-band (I_D/I_G) of Raman spectra. This relationship suggests that I_D/I_G is proportional to the proportion of "boundary" regions within the sample [29]. Subsequent studies have refined this understanding, indicating that L_a corresponds to the average distance between defects in graphite-like materials [30,31]. Despite differing interpretations in these studies, the I_D/I_G ratio is widely accepted as a reliable indicator of disorder in carbon materials. Based on this, we calculated the I_D/I_G ratio from the line scan data, with the results depicted in Fig. 3. It is evident that for both sheared GNP and CNT powders, the I_D/I_G ratio increases with the radial distance from the center, with GNP exhibiting a steeper gradient compared to CNT. For C_{60}, the result presents a different behavior: its I_D/I_G ratio shows no correlation with the radius, remaining randomly distributed around a constant. During the rotation process, there was limited rotational shear at the center of the chamber, and the sample underwent pure translational shear at the edge of the chamber. Measurements of the pressure distribution within the sample chamber confirmed a radial pressure difference (Fig. S1). The uneven distribution of pressure together with the different shear stress states in the sample chamber led to the observation of different I_D/I_G ratios in the GNP and CNT. For C_{60}, the process of collapse was dramatically enhanced by the introduction of extra amount of shear, which could be saturated for this transition when the anvil was rotated by 360°. Therefore, the I_D/I_G of C_{60} remained constant across the sample chamber. This confirms its higher sensitivity to shear stress compared to the other two allotropes.

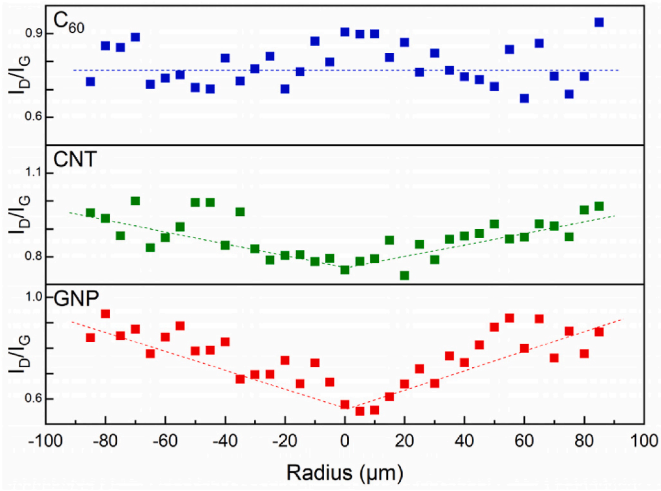

Fig. 3. The evolution of I_D/I_G across the sample chamber of GNP, CNT and C_{60} recovered from high pressure and shear. The dashed straight lines are guide for the eye. (A colour version of this figure can be viewed online.)

TEM characterization was used to further investigate the morphology and microstructure of the samples. The examination of thin sections provided detailed insights into the microstructure changes. For GNP samples quenched from 20 GPa, intact graphene layers were observed (Fig. S4). The measured interlayer spacing is 0.33 nm and consistent with the standard graphite interlayer spacing. CNT that had not been subjected to shear retained their intact fibrous structure, and the voids between the tubes were still observable (Fig. S5). For C_{60} quenched from 20 GPa, crystallinity was partially retained (Fig. S6). After shear, GNP showed preferred orientation (Fig. 4a), CNT lost its tubular character (Fig. 4b) and C_{60} was converted into homogeneous disordered carbon (Fig. 4c). Subsequently, we analyzed the HRTEM images of the samples after shear. From the sheared GNP, numerous disordered nanoclusters were observed, with faults and folds between layers (Fig. 4d). In regions where the layered structure remained relatively intact, an interlayer spacing of approximately 0.35 nm was measured. This spacing is larger than the 0.33 nm interlayer distance of graphite under ambient pressure, indicating that lattice strain was introduced by shear. This observation is consistent with the Raman results, suggesting that compression alone has a minimal impact on GNP, while shear stress plays a critical role in introducing defects and strain. The sheared CNT and C_{60} exhibited a distinct structure transformation. The previously fibrous structure of CNT was no longer discernible. The HRTEM image of the sheared CNT reveals that the tubular structure has disintegrated into curvy graphene fragments (Fig. 4e). The fast Fourier transform (FFT) analyses in Fig. 4d and e indicate that some clusters of sheared GNP and CNT still retain partly ordered and oriented features. However, for C_{60}, it has transformed into an amorphous carbon state (Fig. 4f). The diffuse halo in the FFT patterns (inset) of selected areas confirm the overall amorphous nature of C_{60}, further supporting the transformation observed in the Raman analysis. The SAED patterns for each sample over a larger area demonstrate that the microstructure characteristics revealed by HRTEM and FFT are quite common across extensive regions (Fig. S7).

Shear-induced diamondization in carbon materials has been previously reported [16,18]. To investigate the sp^2 to sp^3 bonding transitions within our samples, we conducted EELS analysis. Fig. 4g presents the EELS spectra of standard graphite alongside those of the three sheared samples. In the high loss region, the features observed at 284 eV and 291 eV correspond to transitions from 1s to π* and σ* states, indicative of sp^2 and sp^3 bonding, respectively [32]. Notably, the EELS spectrum of the sheared C_{60} is smooth and lacks distinct features in the 285 eV–305 eV

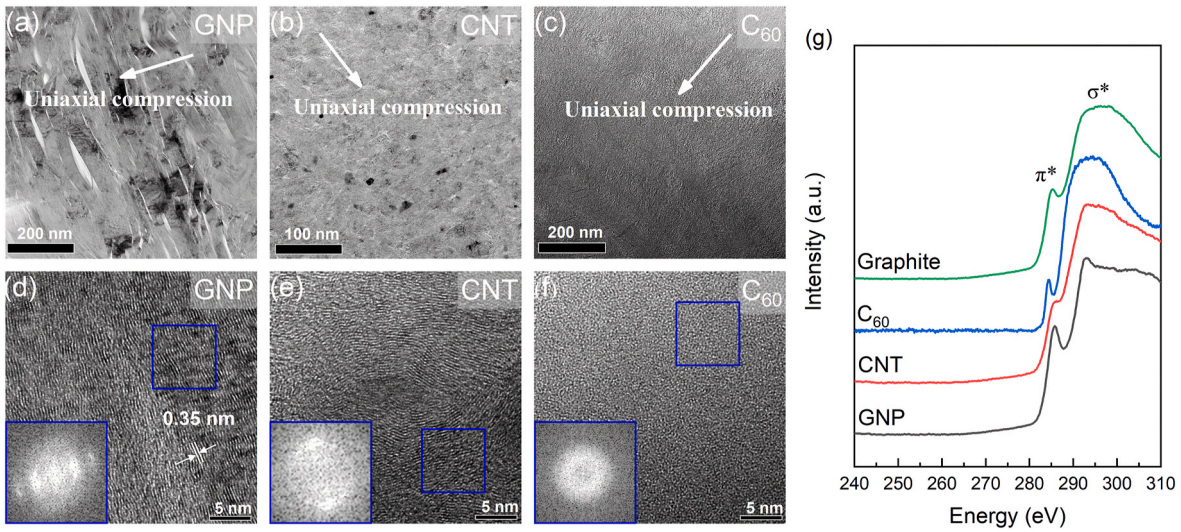

Fig. 4. Morphology and HRTEM images of GNP (a, d), CNT (b, e) and C_{60} (c, f) powders recovered from 20 GPa to 360° of shear. The white arrows represent the direction of the uniaxial compression. All images are taken from the section at position B of the sample chamber. Inset: corresponding FFT results in the blue boxes. (g) Representative EELS spectra of samples recovered from 20 GPa to 360° of shear. (For interpretation of the references to colour in this figure legend, the reader is referred to the Web version of this article.)

range, resembling typical amorphous carbon [33]. A more detailed examination of the EELS spectra allows for a rough estimation of the sp^2 fraction in the probed regions [32–35]. Using standard graphite, which possesses 100 % sp^2, as the reference standard, the sp^2 fraction in the three sheared samples was estimated using equation (1).

$$f = sp^2 / \left(sp^2 + sp^3\right) = \left[I^s_{\pi^*} / \left(I^s_{\pi^*} + I^s_{\sigma^*}\right)\right] / \left[I^g_{\pi^*} / \left(I^g_{\pi^*} + I^g_{\sigma^*}\right)\right] \quad (1)$$

Where f is the fraction of sp^2 in the sample, $I^g_{\pi^*}$ and $I^g_{\sigma^*}$ are the integrated intensities of the 1s→π* and 1s→σ* peaks in the standard sample, respectively, and $I^s_{\pi^*}$ and $I^s_{\sigma^*}$ are the integrated intensities of the 1s→π* and 1s→σ* peaks in our samples, respectively [32]. Detailed results can be found in Table S1, S2 and S3. It can be observed that the average sp^3 fraction of sheared GNP is about 5.71 %. Additionally, it reveals an uneven sp^3 fraction across different positions. In some regions, the sp^3 fraction was calculated to be nearly zero, while in others it reached up to 20.26 %. This indicates the formation of sp^3 bonds between local carbon atoms, consistent with previous reports that observed diamondization in graphite under shear [16,17,36]. In those studies, the transition from graphite to diamond typically occurred through nucleation, resulting in significant spatial variation. For sheared CNT, the average sp^3 fraction is about 15.95 %. In contrast, the sp^3 fraction for C_{60} is approximately 20.84 %. The sp^3 fraction in C_{60} is higher and more uniformly distributed. It may be due to the fact that the carbon bonds of C_{60} have strong buckling, which is more likely to form sp^3 hybridization during the process of breaking and reformation, even at room temperature.

Our experiment transforms carbon with different precursor structures into samples with varying degrees of disorder under extreme conditions. In GNP, the sp^2 bonds are distributed within the graphene plane without any curvature. In CNT, a portion of the sp^2 bonds is curved along the tube walls. In C_{60}, the sp^2 bonds are distributed along the surface of the spherical molecule, with curvature present in all directions around the molecule. The different degree of bond bending in these carbon materials, which has been considered as a source of strain in their geometry and actually changes the nature of the π orbitals [37], could cause their different response to shear stress, resulting in different degree of disorder in the recovered samples. In addition, the collapsibility of C_{60} further contributes to its extreme shear sensitivity.

Previous studies have found that these carbon materials exhibit superhard phases under high pressure, causing damage to diamond anvils [6,11,12]. In our shear experiments with C_{60}, we also observed irreversible damage to the diamond anvils, with the appearance of pronounced ring cracks (see Fig. S8). Some studies on C_{60} have shown that the intermolecular distances shorten under high pressure, and when additional heat is applied, the molecules bond to form dense polymer structures. These polymers are believed to possess exceptional strength and hardness [38–40]. We share the same viewpoint as previous reports regarding the observed cracks in the experiment [11,12]. It indicates that C_{60} exhibits hardness comparable to diamond under high shear stress.

Recently, the preparation and tuning of amorphous materials for specific applications have become a focal point of research. Studying the formation mechanisms of amorphous materials could be significant because they have been proven to possess high strength and hardness. In some high-temperature and high-pressure experiments, C_{60} was used as the carbon source to synthesize amorphous materials with both good hardness and low crystallinity [14,15]. Our experiments also show that C_{60} is highly amorphous after shearing. These results suggest that the coupling of spherical molecules like C_{60} with shear may offer a new approach to preparing amorphous materials. Furthermore, sheared C_{60} could be used as a precursor for the synthesis of nanopolycrystalline diamond [41].

4. Summary and conclusion

In summary, by direct and indirect structural characterizations, we have revealed the disordering behavior of GNP, CNT, and C_{60} fullerene subjected to high pressure and shear. Raman spectroscopy revealed that three samples exhibit different degrees of amorphization under the same rotation degree of diamond anvil, while the C_{60} is more sensitive than GNP and CNT. HRTEM images show that the structures of all three samples were damaged to varying extents after high shear stress treatment. Shearing introduced numerous defects into GNP, with layer faults and folds appearing between the graphitic layers with high lattice strain. The CNT decomposed into severely warped graphene fragments, with the fibrous structure completely destroyed. C_{60} was transformed entirely into uniform amorphous carbon. EELS spectra revealed that shear stress induced a noticeable fraction of sp^3 bond in the carbon nanomaterials at room temperature. This change in carbon atom hybridization suggests that the formation of natural diamonds might be closely related to such processes. Our results highlight the shear-sensitive nature of carbon nanomaterials, provide insights into their mechanical behavior, and

open new avenues for manipulating their properties.

CRediT authorship contribution statement

Yi Yang: Writing – original draft, Writing – review & editing, Data curation, Investigation, Formal analysis, Validation, Methodology. **Mingzhi Yuan:** Writing – review & editing, Validation, Formal analysis, Conceptualization. **Chao Qian:** Data curation. **Chengyu Li:** Data curation. **Yanping Yang:** Data curation. **Xueyan Du:** Data curation. **Hongliang Dong:** Data curation. **Bin Chen:** Writing – review & editing, Investigation, Funding acquisition, Conceptualization, Project administration, Supervision.

Declaration of competing interest

The authors declare that they have no known competing financial interests or personal relationships that could have appeared to influence the work reported in this paper.

Acknowledgments

The authors acknowledge the financial support from Shanghai Key Laboratory of Material Frontiers Research in Extreme Environments (MFree) (No. 22dz2260800), Shanghai Science and Technology Committee (No. 22JC1410300) and National Natural Science Foundation of China (No. 12274101). The authors would like to acknowledge Jiaqi Mo for his assistance in data processing.

Appendix A. Supplementary data

Supplementary data to this article can be found online at https://doi.org/10.1016/j.carbon.2024.119802.

References

[1] C. Lee, X. Wei, J.W. Kysar, J. Hone, Measurement of the elastic properties and intrinsic strength of monolayer graphene, Science 321 (2008) 385–388, https://doi.org/10.1126/science.1157996.
[2] G. Yasin, M. Arif, M. Shakeel, Y. Dun, Y. Zuo, W.Q. Khan, et al., Exploring the nickel–graphene nanocomposite coatings for superior corrosion resistance: manipulating the effect of deposition current density on its morphology, mechanical properties, and erosion-corrosion performance, Adv. Eng. Mater. 20 (7) (2018) 1701166, https://doi.org/10.1002/adem.201701166.
[3] Y. Li, S. Wang, Q. Wang, M. Xing, A comparison study on mechanical properties of polymer composites reinforced by carbon nanotube and graphene sheet, Composites, Part B 133 (2018) 35–41, https://doi.org/10.1016/j.compositesb.2017.09.024.
[4] L. Sun, F. Banhart, A.V. Krasheninnikov, J.A. Rodriguez-Manzo, M. Terrones, P. M. Ajayan, Carbon nanotube as high-pressure cylinders and nanoextruders, Science 312 (5777) (2006) 1199–1202, https://doi.org/10.1126/science.1124594.
[5] L. Pizzagalli, Mechanical properties of C_{60} at finite temperature from first-principles calculations, Diam. Relat. Mater. 123 (2022) 108870, https://doi.org/10.1016/j.diamond.2022.108870.
[6] W.L. Mao, H.K. Mao, P.J. Eng, T.P. Trainor, M. Newville, C. Kao, et al., Bonding changes in compressed superhard graphite, Science 302 (5644) (2003) 425–427, https://doi.org/10.1126/science.108971.
[7] M. Yuan, R.A. Susilo, S. Li, J. Feng, V. Benavides, J. Chen, et al., Fragmentation and structural transitions of few-layer graphene under high shear stress, Appl. Phys. Lett. 118 (21) (2021) 213101, https://doi.org/10.1063/5.0049592.
[8] Z. Wang, Y. Zhao, K. Tait, X. Liao, D. Schiferl, C. Zha, et al., A quenchable superhard carbon phase synthesized by cold compression of carbon nanotube, Proc. Natl. Acad. Sci. U.S.A. 101 (38) (2004) 13699–13702, https://doi.org/10.1073/pnas.0405877101.
[9] C. Chen, Y. Lin, W. Zhou, M. Gong, Z. He, F. Shi, et al., Sub-10-nm graphene nanoribbons with atomically smooth edges from squashed carbon nanotube, Nat. Electron. 4 (2021) 653–663, https://doi.org/10.1038/s41928-021-00633-6.
[10] V.D. Blank, B.A. Kulnitskiy, Y.V. Tatyanin, Structural studies of high pressure phases of C_{60}, Phys. Lett. 204 (2) (1995) 151–154, https://doi.org/10.1016/0375-9601(95)00429-7.
[11] V.D. Blank, M. Popov, S.G. Buga, V. Davydov, V.N. Denisov, A.N. Ivlev, et al., Is C_{60} fullerite harder than diamond? Phys. Lett. 188 (3) (1994) 281–286, https://doi.org/10.1016/0375-9601(94)90451-0.
[12] V.D. Blank, S.G. Buga, N.R. Serebryanaya, V.N. Denisov, G.A. Dubitsky, A.N. Ivlev, et al., Ultrahard and superhard carbon phases produced from C_{60} by heating at high pressure: structural and Raman studies, Phys. Lett. 205 (2–3) (1995) 208–216, https://doi.org/10.1016/0375-9601(95)00564-J.
[13] A. Lundin, B. Sundqvist, P. Skoglund, Å. Fransson, S. Pettersson, Compressibility, Specific heat capacity, and Grüneisen parameter for C_{60}/C_{70}, Solid State Commun. 84 (9) (1992) 879–883, https://doi.org/10.1016/0038-1098(92)90451-E.
[14] H. Tang, X. Yuan, Y. Cheng, H. Fei, F. Liu, T. Liang, et al., Synthesis of paracrystalline diamond, Nature 599 (7886) (2021) 605–610, https://doi.org/10.1038/s41586-021-04122-w.
[15] S. Zhang, Y. Wu, K. Luo, B. Liu, Y. Shu, Y. Zhang, et al., Narrow-gap, semiconducting, superhard amorphous carbon with high toughness, derived from C_{60} fullerene, Cell Rep. Phys. Sci. 2 (9) (2021), https://doi.org/10.1016/j.xcrp.2021.100575.
[16] Y. Gao, Y. Ma, Q. An, V. Levitas, Y. Zhang, B. Feng, et al., Shear driven formation of nano-diamonds at sub-gigapascals and 300 K, Carbon 146 (2019) 364–368, https://doi.org/10.1016/j.carbon.2019.02.012.
[17] J. Dong, Z. Yao, M. Yao, R. Li, K. Hu, L. Zhu, et al., Decompression-induced diamond formation from graphite sheared under pressure, Phys. Rev. Lett. 124 (6) (2020) 065701, https://doi.org/10.1103/PhysRevLett.124.065701.
[18] S. Wong, T.B. Shiell, B.A. Cook, J.E. Bradby, D.R. McKenzie, D.G. McCulloch, The shear-driven transformation mechanism from glassy carbon to hexagonal diamond, Carbon 142 (2019) 475–481, https://doi.org/10.1016/j.carbon.2018.10.080.
[19] Y. Akahama, H. Kawamura, Pressure calibration of diamond anvil Raman gauge to 410 GPa, J. Phys.: Conf. Ser. 215 (2010) 012195, https://doi.org/10.1088/1742-6596/215/1/012195.
[20] J.H. Nguyen, M.B. Kruger, R. Jeanloz, Amorphization and a new polymorph of carbon synthesized from C_{60}, Solid State Commun. 88 (9) (1993) 719–721, https://doi.org/10.1016/0038-1098(93)90631-V.
[21] J. Haines, J.M. Leger, An X-ray diffraction study of C_{60} up to 28 GPa, Solid State Commun. 90 (6) (1994) 361–363, https://doi.org/10.1016/0038-1098(94)90799-4.
[22] A.C. Ferrari, J. Robertson, Interpretation of Raman spectra of disordered and amorphous carbon, Phys. Rev. B 61 (20) (1999) 14095, https://doi.org/10.1103/PhysRevB.61.14095.
[23] E.F. Antunes, A.O. Lobo, E.J. Corat, V.J. Trava-Airoldi, Influence of diameter in the Raman spectra of aligned multi-walled carbon nanotube, Carbon 45 (2007) 913–921, https://doi.org/10.1016/j.carbon.2007.01.003.
[24] S.M. Clark, K.J. Jeon, J.Y. Chen, C.S. Yoo, Few-layer graphene under high pressure: Raman and X-ray diffraction studies, Solid State Commun. 154 (2013) 15–18, https://doi.org/10.1016/j.ssc.2012.10.002.
[25] I. Loa, Raman spectroscopy on carbon nanotubes at high pressure, J. Raman Spectrosc. 34 (7–8) (2003) 611–627, https://doi.org/10.1002/jrs.1035.
[26] K.P. Meletov, D. Christofilos, G.A. Kourouklis, S. Ves, Pressure induced phase transitions in C_{60} single crystals,, Chem. Phys. Lett. 236 (3) (1995) 265–270, https://doi.org/10.1016/0009-2614(95)00205-I.
[27] W. Qiu, S. Chowdhury, R. Hammer, N. Velisavljevic, P. Baker, Y.K. Vohra, Physical and mechanical properties of C_{60} under high pressures and high temperatures, High Pres. Res. 26 (3) (2006) 175–183, https://doi.org/10.1080/08957950600834792.
[28] P. Botella, X. Devaux, M. Dossot, V. Garashchenko, J.C. Beltzung, A.V. Soldatov, et al., Single-walled carbon nanotube shock-compressed to 0.5 mbar, Phys. Status Solidi B 254 (11) (2017) 1700315, https://doi.org/10.1002/pssb.201700315.
[29] F. Tuinstra, J.L. Koenig, Raman spectrum of graphite, J. Chem. Phys. 53 (3) (1970) 1126–1130, https://doi.org/10.1063/1.1674108.
[30] A. Jorio, E.H.M. Ferreira, M.V.O. Stavale, C.A. Achete, R.B. Capaz, Measuring disorder in graphene with the G and D bands, Phys. Status Solidi B 247 (11–12) (2010) 2980–2982, https://doi.org/10.1002/pssb.201000247.
[31] S. Eigler, C. Dotzer, A. Hirsch, Visualization of defect densities in reduced graphene oxide, Carbon 50 (2012) 3666–3673, https://doi.org/10.1016/j.carbon.2012.03.039.
[32] S. Urbonaite, S. Wachtmeister, C. Mirguet, E. Coronel, W.Y. Zou, S. Csillag, et al., EELS studies of carbide derived carbons, Carbon 45 (10) (2007) 2047–2053, https://doi.org/10.1016/j.carbon.2007.05.022.
[33] H. Daniels, R. Brydson, B. Rand, A. Brown, Investigating carbonization and graphitization using electron energy loss spectroscopy (EELS) in the transmission electron microscope (TEM), Philos. Mag. A 87 (27) (2007) 4073–4092, https://doi.org/10.1080/14786430701394041.
[34] B.W. Reed, M. Sarkaya, TEM/EELS analysis of heat-treated carbon nanotube experimental techniques, Microscopy 51 (2002) S97–S105, https://doi.org/10.1093/jmicro/51.Supplement.S97.
[35] S.D. Berger, D.R. McKenzie, P.J. Martin, EELS analysis of vacuum arc-deposited diamond-like films, Phil. Mag. Lett. 57 (6) (1988) 285–290, https://doi.org/10.1080/09500838808214715.
[36] S. Paul, K. Momeni, V.I. Levitas, Shear-induced diamondization of multilayer graphene structures: a computational study, Carbon 167 (2020) 140–147, https://doi.org/10.1016/j.carbon.2020.05.038.
[37] R.C. Haddon, Chemistry of the fullerenes: the manifestation of strain in a class of continuous aromatic molecules, Science 261 (5128) (1993) 1545–1550. https://www.science.org/doi/abs/10.1126/science.261.5128.1545.
[38] B. Sundqvist, Polymeric fullerene phases formed under pressure, Struct. Prop. 109 (2004) 85–126, https://doi.org/10.1007/b94380.
[39] V.D. Blank, S.G. Buga, N.R. Serebryanaya, G.A. Dubitsky, S.N. Sulyanov, M. Y. Popov, et al., Phase transformations in solid C_{60} at high-pressure-high-

temperature treatment and the structure of 3D polymerized fullerites, Phys. Lett. 220 (1–3) (1996) 149–157, https://doi.org/10.1016/0375-9601(96)00483-5.
[40] V.D. Blank, S.G. Buga, G.A. Dubitsky, N.R. Serebryanaya, M.Y. Popov, B. Sundqvist, High-pressure polymerized phases of C_{60}, Carbon 36 (4) (1998) 319–343, https://doi.org/10.1016/S0008-6223(97)00234-0.
[41] T. Irifune, A. Kurio, S. Sakamoto, T. Inoue, H. Sumiya, Ultrahard polycrystalline diamond from graphite, Nature 421 (2003) 599–600, https://doi.org/10.1038/421806b.